

# Template-Free Synthesis of Mesoporous N-doped SrTiO<sub>3</sub> with Visible-Light-Driven Photocatalytic Activity

Fei Zou<sup>a,b,e</sup>, Zheng Jiang<sup>a,c,\*</sup>, Xiaoqin Qin<sup>a,d</sup>, Yongxiang Zhao<sup>d</sup>, Luyun Jiang<sup>a</sup>, Jinfang Zhi<sup>b</sup>, Tiancun Xiao<sup>a</sup>, Peter P. Edwards<sup>a,\*</sup>

<sup>a</sup> Department of Chemistry, Inorganic Chemistry Laboratory, University of Oxford, Oxford, OX1 3QR, UK;

<sup>b</sup> Key Laboratory of Photochemical Conversion and Optoelectronic Materials, Technical Institute of Physics and Chemistry, 29 Zhongguancun East Road, Haidian District, Beijing, 100190, China

<sup>c</sup> Environment and Sustainability Institute, University of Exeter, Cornwall Campus, Penryn, Cornwall, TR10, 9EZ, UK

<sup>d</sup> School of Chemistry and Chemical Engineering, Shanxi University, Taiyuan 030006, China

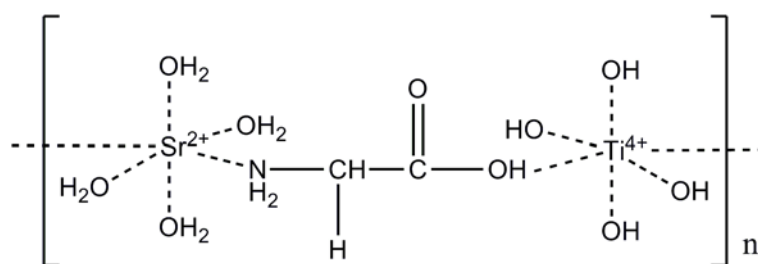
<sup>e</sup> Graduate School of Chinese Academy of Sciences, Beijing 100864, China

Corresponding authors: Dr. Zheng Jiang, Tel: +44 (0) 1326 255795, Email: [zhjiang76@hotmail.com](mailto:zhjiang76@hotmail.com);

Prof. Peter P. Edwards, Tel: 44(0)1865 272646, Email: [peter.edwards@chem.ox.ac.uk](mailto:peter.edwards@chem.ox.ac.uk)

## Part I. Experimental

### 1. Synthesis of pure SrTiO<sub>3</sub> (STO) and N-doped SrTiO<sub>3</sub> (STON)



Scheme S1. The molecular structure of metal-glycine complexes

All chemicals involved were purchased from Sigma Aldrich and used as received without further purification. Glycine was chosen as coordinate agent to form complex compound with Sr<sup>2+</sup> and Ti<sup>4+</sup> (Scheme S1) because most amino acids are able to form stable complexes with alkaline earth and transition metals<sup>1,2</sup>. In a typical synthesis, 5 mL aqueous solution containing 10 mmol glycine and 10 mmol Sr(NO<sub>3</sub>)<sub>2</sub> were added drop by drop into 40 mL ethanol solution containing 10 mmol of tetrabutyl titanate (TBT, C<sub>16</sub>H<sub>36</sub>O<sub>4</sub>Ti) and 2 mL glacial acetic acid under rigorous stirring, following with natural

evaporation and drying in a fume hood. The obtained dry gel was ground and calcinated at 550 °C/2h, with a temperature ramp of 10 °C/min, to obtain the meso-STON. Pure SrTiO<sub>3</sub> was prepared via the same procedure mentioned above except for without glycine added.

## 2. Characterization.

X-ray powder diffraction data of the prepared samples were recorded on a PANalytical X'Pert PRO at 40 KV and 30mA. Transmission electron microscopy (TEM) was performed with a Jeol JEM- 2010 electron microscope operated at 200 kV.

Nitrogen adsorption-desorption isotherms were measured on a Micromeritics ASAP 2010 at 77 K with samples degassed at 373 K for 5 h. Pore size distributions were calculated from the adsorption isotherm using the BJH method and the BET surface area from a relative pressure of 0.03-0.2.

X-Ray photoelectron spectroscopy (XPS) was performed using a Perkin-Elmer RBD upgraded PHI-5000C ESCA system with monochromatic Mg-Ka excitation and a charge neutralizer was used to investigate the surface electronic states of the N doped samples. All the binding energies were calibrated with contaminant C 1s at binding energy of 284.8 eV.

The UV-vis diffuse reflectance spectra (DRS) were measured using a UV-Vis DRS (Cary, UV-5000) within a wavelength range of 200-800nm at room temperature. Fourier transform infra red spectra (FTIR) were carried out using diffused reflectance model on a Varian FTS-7000 Fourier Transform Infrared Spectrometers.

The electron spin resonance (ESR) spectra were recorded on a Magnetech Miniscope MS200 EMX spectrometer operating at 100 KHz magnetic field modulation. The amplitude was normalized by  $I/I_{\max}$ . Simulation of ESR spectra was performed using the EASYSPIN software package.<sup>3</sup>

## 3. Photocatalytic Degradation of Dyes under Visible Light Irradiation

The photocatalytic abilities of the STO and STON were evaluated by measuring the degradation of Rhodamine B (RhB), Methylene Blue (MB) and Methyl Orange (MO) aqueous solutions, respectively. A 300W Xenon lamp (PLS-SXE300, Beijing TrustTech) was used as the visible-light source with UV-cutoff filters (UVCUT420, Beijing TrustTech). In the typical photocatalytic experiment, 0.1g catalyst was dispersed into 100mL of dye aqueous solution (10 ppm). Prior to irradiation, the

suspensions were stirred in dark for 1.0 hour to ensure the absorption-desorption equilibrium of the dye on the surface of catalysts. During the light irradiation, approximately 3.0 mL of suspension was collected every 20 minutes. After removal the photocatalyst particles from the suspension by centrifuge, the supernatant solutions were analyzed by a Perkin-Elmer Lambda 750S UV-visible spectrophotometer. Lambert-Beer rule was applied at the characteristic absorbance bands of dyes, RhB at 553nm, MB 665 nm and MO 463 nm, to determine their concentration changes.

## Part II. Discussion

### 1. XRD patterns of STO and STON

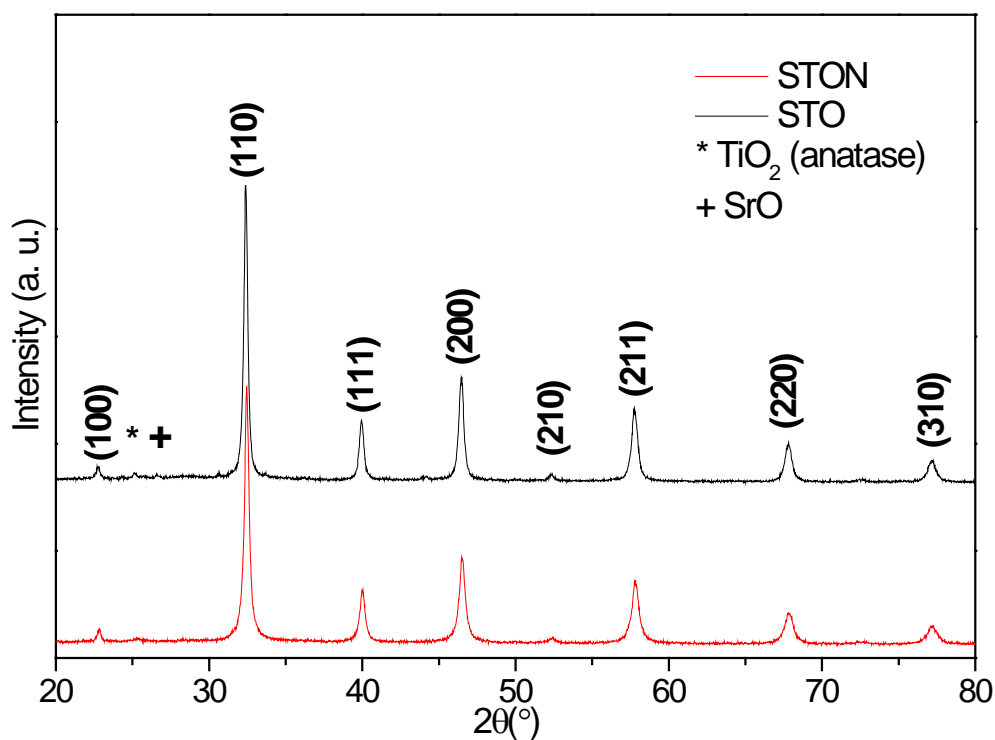


**Fig. S1** (A) Wide-angle XRD patterns of STO and STON samples

[Fig.S1](#) shows the wide angle XRD patterns of the STO and STON samples, where the Bragg peaks can be well indexed to the perovskite-structured  $\text{SrTiO}_3$  (JCPDS: 74-1296). The lattice parameter of STON is slightly smaller than that of STO, while the crystallite size of STON (46.4 nm) is nearly half of that of STO (82.5 nm). STON possessed more pure perovskite phase than the STO sample, which comprised of trace amounts of anatase  $\text{TiO}_2$  (JCPDS: 71-1169) and SrO (JCPDS: 65-2652)<sup>4-6</sup>. It is previously reported the addition of chelate agent, such as acetylacetonate and ethylene glycol, may greatly reduce the impurities (SrO and/or  $\text{TiO}_2$ ) in the chemical synthesis of

STO<sup>7</sup>.

## 2. TEM and N<sub>2</sub>-isotherm of STO

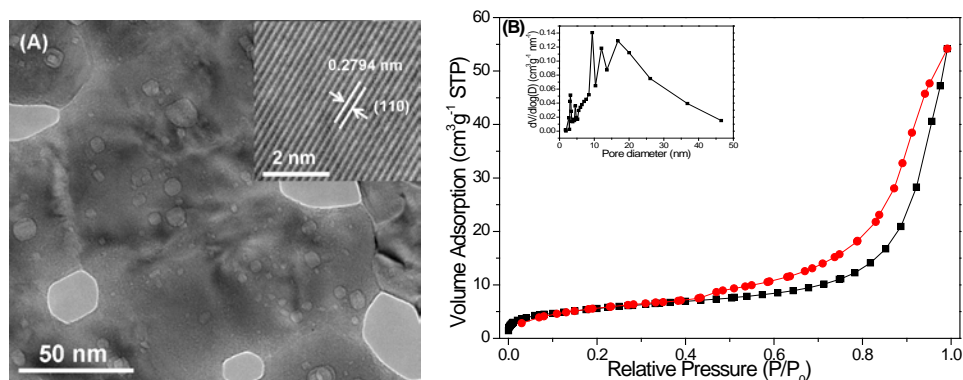


Fig. S2 Bright-field TEM and HRTEM (inset) images (A) and N<sub>2</sub> adsorption-desorption isotherm (B) of STO. The inset of Fig S2(B) is the pore-size distribution of STO sample.

The TEM image in Fig.S2(A) shows the STO sample comprises of poor porosity with irregular pore shape and less uniform sizes. The HRTEM image inserted in Fig.S2 (A) reveals that the walls of the mesopores are also single crystal perovskite STO. The labeled lattice distance is consistent with (110) diffraction obtained from XRD tests (Fig.S1).

The porosity of the STO sample was revealed by the observed Type-II N<sub>2</sub> adsorption-desorption isotherm and type-H3 hysteresis loop of the meso-STON (Fig.S2B) suggest it possesses “cylinder-like” mesopores<sup>8</sup>. The pore size distribution of the mesoporous is quite broad as shown in the inset plot of Fig.S2 (B).

## 3. Ti 2p XPS of STO and STON

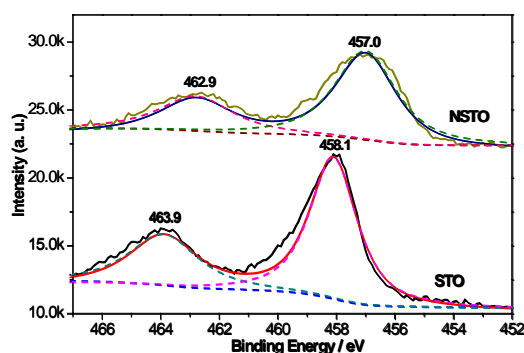


Figure S3. Ti 2p XPS of STO and STON

The detailed XPS spectra of Ti 2p around 460 eV are shown in Fig. S3. The XPS spectrum for Ti exhibits two signals of Ti 2p<sub>3/2</sub> and Ti 2p<sub>1/2</sub>. The binding energy of the Ti 2p<sub>3/2</sub> and Ti 2p<sub>1/2</sub> for STON (457.9, 463.1 eV) are lower than that for pure STO (459.4, 465.4 eV). It is supposed that the red shift of the binding energy of Ti 2p is induced by the N-doping which can reduce Ti<sup>4+</sup> to Ti<sup>3+</sup>.<sup>8</sup>

#### 4. Photodegradation of RhB of STO and STON under simulated solar irradiation

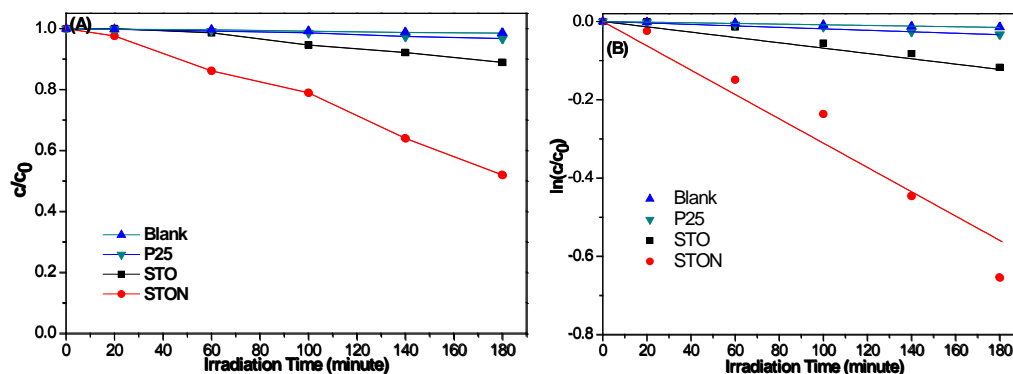


Figure S4. photodegradation of RhB under visible-light irradiation(A) and their corresponding plot of  $\ln(C/C_0)$  versus irradiation time (B).

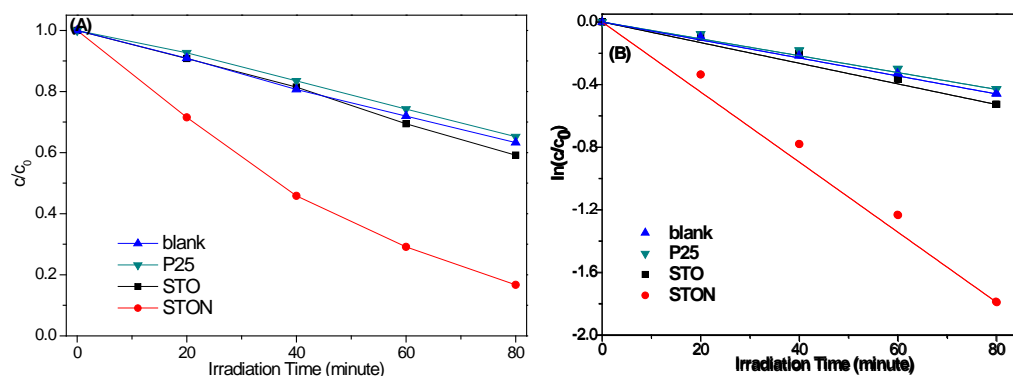


Figure S5. photodegradation of MB under visible-light irradiation(A) and their corresponding plot of  $\ln(C/C_0)$  versus irradiation time (B).

Fig. S4 show the plot of  $\ln(C/C_0)$  versus irradiation time for the photodegradation of RhB over STO and STON under visible-light irradiation. Fig. S5 shows the photodegradation of MB over STO and STON under visible-light irradiation (A) and their corresponding plot of  $\ln(C/C_0)$  versus irradiation time (B). The apparent RhB and MB photodegradation rates under visible-light irradiation listed in Table S1 are derived from pseudo-first-order model,  $\ln(C/C_0)$ , where C and  $C_0$  are the concentration of RhB (or MB) at time t and 0, respectively, and k is pseudo-first-order reaction rate constant.<sup>9</sup>

**Table S1. Lattice parameters, crystallite size, pore size, BET surface area,  $E_g$  and photoreaction rate constants ( $k_{\text{RhB}}$ ) of STO and STON samples under visible-light irradiation.**

Photocatalyst	a=b=c (Å) <sup>a</sup>	Crystallite size (nm) <sup>b</sup>	Dp (nm)	SSA <sup>c</sup> (m <sup>2</sup> /g)	$E_g$ (eV) <sup>d</sup>	$k$ (min <sup>-1</sup> ) <sup>e</sup>	
						MB	RhB
STO	3.908	82.5	12.4	19.5	3.2	0.0066	0.0007
STON	3.903	46.4	4.0	52.3	2.9	0.0224	0.0031
TiO <sub>2</sub> P25	-	-	-	-	3.2	0.0054	0.0002

Note: <sup>a</sup> lattice parameters; <sup>b</sup> calculated from the Debye-Scherrer equation; <sup>c</sup> SSA refers to BET specific surface area; <sup>d</sup>  $E_g$  was derived from  $E_g = 1239.8/\lambda_g$ , where  $\lambda_g$  is the absorption edge in the UV-Vis spectra; <sup>e</sup> apparent kinetics constants of photocatalytic reactions under full arc and visible-light irradiations.

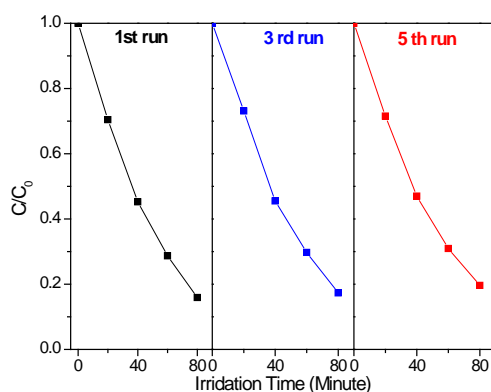


Figure S6. Lifetime of visible-light photo-degradation MB over STON under visible-light irradiation.

The photodegradation of MB was cycled 5 times under the same condition to used to investigate the stability of the meso-STON. In the cycling tests, the used meso-STON were centrifuged after completing the photocatalysis reaction and re-dispersed into 100 mL MB solution for the next round of repeated test. As shown in Fig. S6, meso-STON exhibited very similar photocatalysis activity in 5 times of repeated tests, revealing it is a highly stable photocatalyst.

## References

1. M. F. Bush, J. Oomens, R. J. Saykally and E. R. Williams, *Journal of the American Chemical Society*, 2008, **130**, 6463-6471.
2. E. F. Strittmatter, A. S. Lemoff and E. R. Williams, *Journal of Physical Chemistry A*, 2000, **104**, 9793-9796.
3. S. Stoll and A. Schweiger, *Journal of Magnetic Resonance*, 2006, **178**, 42-55.
4. U. Sulaeman, S. Yin and T. Sato, *Journal of Nanomaterials*, 2010, **2010**.
5. J. Wang, H. Li, H. Li, S. Yin and T. Sato, *Solid State Sciences*, 2009, **11**, 182-188.
6. S. Ouyang, H. Tong, N. Umezawa, J. Cao, P. Li, Y. Bi, Y. Zhang and J. Ye, *Journal of the American Chemical Society*, 2012, **134**, 1974-1977.
7. X. X. Fan, Y. Wang, X. Y. Chen, L. Gao, W. J. Luo, Y. P. Yuan, Z. S. Li, T. Yu, J. H. Zhu and Z. G. Zou, *Chemistry of Materials*, 2010, **22**, 1276-1278.
8. X. B. Chen and C. Burda, *Journal of Physical Chemistry B*, 2004, **108**, 15446-15449.
9. L. Kong, Z. Jiang, T. C. Xiao, L. F. Lu, M. O. Jones and P. P. Edwards, *Chemical Communications*, 2011, **47**, 5512-5514.